Supplementary Information for "DynQual v1.0: A high-resolution global surface water quality model"

Edward R. Jones[1,*], Marc F.P Bierkens[1,2], Niko Wanders[1], Edwin H. Sutanudjaja[1], Ludovicus P.H van Beek[1], Michelle T.H. van Vliet[1]

[1]Department of Physical Geography, Faculty of Geosciences, Utrecht University, Utrecht, The Netherlands.

[2]Deltares, Unit Soil and Groundwater Systems, Utrecht, The Netherlands

* Correspondence to: e.r.jones@uu.nl

1. Pollutant loadings

Pollutant loadings can be either be: 1) prescribed by the user directly; or 2) calculated within the DynQual run by providing simple input data. When loadings are prescribed directly to the model, the user is only required to provide input files on the total (i.e. combined) pollutant loadings of TDS (in g day^{-1}), BOD (in g day^{-1}), FC (in 10^6 cfu day^{-1}) and Tw (in MW). Conversely, when pollutant loadings are calculated within the DynQual, a variety of input data is required to reflect both pollutant emissions from sectoral activities and the transmission of pollution to the environment (Jones et al., 2022). The subsequent routing of pollutants through the stream network and the calculation of in-stream concentrations follows the same approach in both configurations.

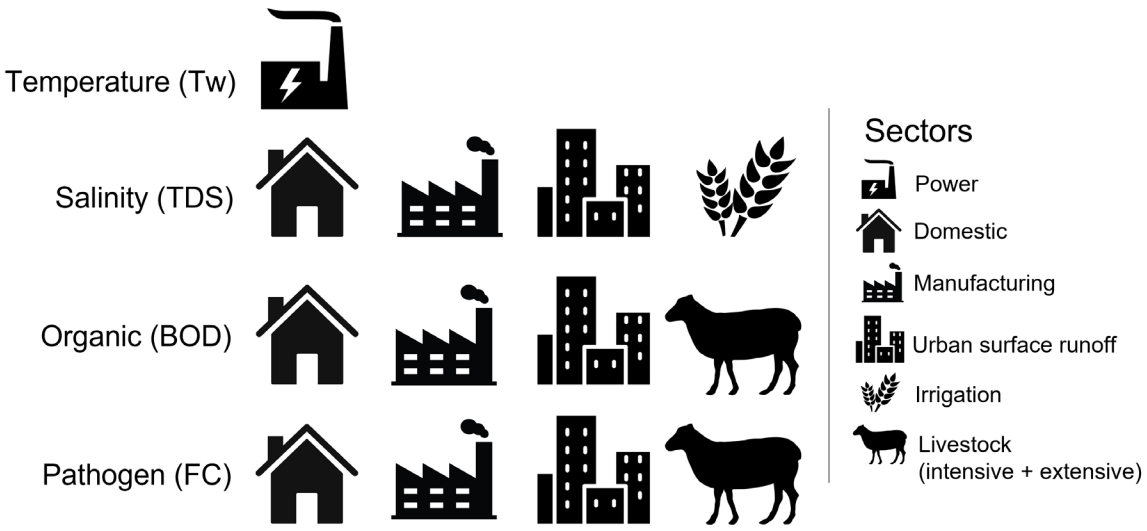

Figure S1. Simplified approach for pollutant routing and the calculation of in-stream concentrations.

The following section describes the approach used and assumptions made for calculating pollutant loadings dynamically within a DynQual model run. DynQual considers pollutant emissions from five distinct sectors (domestic, manufacturing, livestock, irrigation and thermo-electric power generation) and from urban surface runoff (Figure S1). The prevalence of wastewater collection and treatment, combined with their associated pollutant removal efficiencies, are key factors controlling subsequent delivery of pollution to surface waters (Jones et al., 2022). For detailed information about the development of grid cell specific wastewater treatment practices and their inclusion in DynQual, we refer to the previous work (Jones et al., 2021; Jones et al., 2022).

1.1 Domestic

$$L_{dom,i,n} = Pop_n \cdot E_{dom,i,n} \cdot (1 - R_{dom,i,n}) \quad \textbf{[1]}$$

Pollutant loadings from the domestic sector ($L_{dom,i,n}$) are calculated by multiplying the population (Pop_n) in gridcell *n* by a regional-specific per capita excretion rate ($E_{dom,i,n}$) of pollutant *i* (TDS and BOD in g $capita^{-1}$ day^{-1}; FC in cfu $capita^{-1}$ day^{-1}) [1]. Pollutant loadings are abated based upon gridcell specific domestic wastewater collection and treatment practices, represented by $R_{dom,i,n}$, which depends upon the wastewater pathway(s) in gridcell *n* and the pathway-specific removal efficiency of pollutant *i* (Jones et al., 2021; Jones et al., 2022).

Gridded population data at 5 arc-minutes was obtained from ISIMIP3a (Lange and Geiger, 2020). Per capita pollutant loadings are prescribed per water quality constituent at the regional scale (Table S1). Per capita excretion rates of BOD and FC vary at the regional level due to differences in diet, climate and health status (Williams et al., 2012; UNEP, 2016). Conversely, due to a lack of more detailed data, an average global value for per capita excretion of TDS was used. Pollutant loadings per capita are based on extensive literature research conducted for previous global water quality modelling studies (UNEP, 2016; Van Vliet et al., 2021) and are assumed to remain constant throughout the study period.

Table S1. Domestic sector total dissolved solids (TDS), biological oxygen demand (BOD) and fecal coliform (FC) loadings per geographic region.

Geographic Region	Domestic		
	TDS (g day^{-1} capita^{-1})*	BOD (g day^{-1} capita^{-1})*	FC (cfu day^{-1} capita^{-1})*
North America	100	65	$1.3 \cdot 10^{10}$
Latin America & Caribbean	100	56	$1.4 \cdot 10^{10}$
Western Europe	100	60	$1.3 \cdot 10^{10}$
Middle East & North Africa	100	45	$1.8 \cdot 10^{10}$
Sub-Saharan Africa	100	37	$4.7 \cdot 10^{9}$
Southern Asia	100	40	$1.9 \cdot 10^{10}$
Eastern Europe & Central Asia	100	50	$1.6 \cdot 10^{10}$
East Asia & Pacific	100	50	$1.6 \cdot 10^{10}$

*as per UNEP (2016) and van Vliet et al. (2021); **as per UNEP (2016) and Williams et al., (2012); ***as per UNEP (2016) and Reder et al., (2015)

1.2 Manufacturing

$$L_{man,i,n} = WW_{man,n} \cdot C_{man,i,n} \cdot (1 - R_{man,i,n}) \quad \textbf{[2]}$$

Pollutant loadings from the manufacturing sector ($L_{man,i,n}$) are calculated by multiplying the manufacturing wastewater flows (return flows) in gridcell *n* ($WW_{man,n}$ in m^3 s^{-1}) by a mean manufacturing effluent concentration ($C_{man,i,n}$) for pollutant *i* (TDS and BOD in mg l^{-1}; FC in cfu l^{-1}) [2]. Pollutant loadings are abated based upon gridcell-specific manufacturing wastewater collection and treatment practices, represented by $R_{man,i,n}$ which depends upon the wastewater pathway(s) in gridcell *n* and the pathway-specific removal efficiency of pollutant *i* (Jones et al., 2021; Jones et al., 2022).

As PCR-GLOBWB2 does not distinguish explicitly between the manufacturing and thermoelectric power sectors (lumped together as the "industrial" sector), we estimate the percentage of total industrial flows that originate specifically from manufacturing activities and apply this to PCR-GLOBWB2 simulated industrial return flows at the country level. To make this distinction, we subtract power return flows derived from an external source (Lohrmann et al., 2019) from PCR-GLOBWB2 industrial return flows, to provide an estimate of manufacturing return flows. We further

cross-checked these estimated manufacturing return flows against a spatially-explicit municipal wastewater dataset (Jones et al., 2021).

Lacking more detailed information regarding both the specific manufacturing processes and the associated effluent quality, globally consistent effluent concentrations are applied for all manufacturing return flows worldwide (Table S2), consistent with previous work (UNEP, 2016; Van Vliet et al., 2021). Mean effluent concentrations are derived from literature review and are assumed to remain constant throughout the study period.

Table S2. Manufacturing sector total dissolved solids (TDS), biological oxygen demand (BOD) and fecal coliform (FC) effluent concentrations.

	TDS (mg l^{-1})*	**BOD (mg l^{-1})***	**FC (cfu l^{-1})***
Global	3000	400	$3.55 \cdot 10^8$

*as per UNEP (2016) and van Vliet et al. (2021)

1.3 Urban surface runoff

$$L_{urb,i,n} = RF_{USR,n} \cdot C_{USR,i,n} \cdot (1 - R_{USR,i,n})$$

[3]

Pollutant loadings from urban surface runoff ($L_{urb,i,n}$) are calculated by multiplying urban surface return flows ($RF_{USR,n}$ in $m^3\ s^{-1}$) in gridcell *n* by a mean urban runoff effluent concentration ($C_{USR,i,n}$) for pollutant *i* (TDS and BOD in mg l^{-1}; FC in cfu l^{-1}) [3]. Pollutant loadings are abated based upon gridcell-specific wastewater collection and treatment practices, represented by $R_{USR,i,n}$which depends upon the wastewater pathway(s) in gridcell *n* and the pathway-specific removal efficiency of pollutant *i* (Jones et al., 2021; Jones et al., 2022)

Urban surface runoff flows are simulated within PCR-GLOBWB2 (Sutanudjaja et al., 2018), calculated by multiplying the fraction of the gridcell that is urban by the simulated surface runoff. Mean urban surface runoff pollutant concentrations are taken from existing work (UNEP, 2016), based on extensive literature review. TDS and BOD concentrations vary at the regional level whereas, lacking detailed data, FC is assumed to be constant across all regions (Table S3). Mean urban surface runoff concentrations are assumed to remain constant throughout the study period.

Table S3. Urban surface runoff total dissolved solids (TDS), biological oxygen demand (BOD) and fecal coliform (FC) mean concentrations per geographic region.

Region	Urban surface runoff		
	TDS (mg l^{-1})*	BOD (mg l^{-1})*	FC (cfu l^{-1})*
North America	205	12	$1 \cdot 10^6$
Latin America & Caribbean	205	12	$1 \cdot 10^6$
Western Europe	205	12	$1 \cdot 10^6$
Middle East & North Africa	212	19	$1 \cdot 10^6$
Sub-Saharan Africa	178	62	$1 \cdot 10^6$
Southern Asia	246	105	$1 \cdot 10^6$
Eastern Europe & Central Asia	246	19	$1 \cdot 10^6$
East Asia & Pacific	246	105	$1 \cdot 10^6$

*as per UNEP (2016)

1.4 Livestock

For calculating pollutant loadings from the livestock sector, the sector is sub-divided into intensive and extensive systems based on livestock population density. For defining intensive livestock systems, a minimum threshold density of 25 livestock units per km^2 was set with one livestock unit equivalent to ~250kg (1 bovine) (Wen et al., 2017; Vigiak et al., 2019). Average animal mass equivalent coefficients were taken from literature (Robinson et al., 2011; Wen et al., 2017) to convert this threshold density into a livestock-type specific threshold density per km^2 (Wen et al., 2017; Vigiak et al., 2019). Gridcells exceeding this threshold density (per livestock type) were designated as intensive livestock systems, whereas gridcells below this threshold were designated as extensive livestock systems.

The distinction between intensive and extensive livestock systems is made to account for the differences in the paths by which livestock waste (manure) enters the stream network, namely whether there is transportation by surface runoff (for extensive systems) or whether there is collection (and potentially subsequent treatment) of livestock waste (for intensive systems). Abation of collected livestock waste is all assumed to be at the same level as secondary treatment in line with Wen et al (2017) and occurs only in gridcells where municipal wastewater treatment is also occurring. The waste is subsequently assumed to be spread to land as manure and transported to surface water via surface runoff. This approach for calculating pollutant loadings from the livestock sector is line with previous work (Wen et al., 2017; Vigiak et al., 2019).

Table S4. Threshold density for designation of livestock activities as intensive systems, per livestock type.

Livestock type	Animal mass equivalent coefficient*	Threshold density (stock km^{-2})
Buffalo	1	25
Chicken	0.01	2500
Cow	1	25
Duck	0.01	2500
Goat	0.1	250
Horse	1	25
Pig	0.3	83
Sheep	0.1	250

* as per Robinson et al. (2011) and Wen et al. (2017)

Pollutant loadings from the livestock sector are calculated as per Eq. [4], in line with the previous approaches for calculating pollutant loadings from intensive (Wen et al., 2017; Vigiak et al., 2019) and extensive (Van Vliet et al., 2021) livestock systems:

$$L_{intLiv,i,n} = \Sigma_y \left(LivPop_{y,n} * E_{liv,y,i,n}\right) \cdot (1 - R_{liv,i,n}) \cdot s_n$$

$$L_{extLiv,i,n} = \Sigma_y \left(LivPop_{y,n} \cdot E_{liv,y,i,n}\right) \cdot s_n \quad \textbf{[4]}$$

Where: $L_{intLiv,i,n}$ and $L_{extLiv,i,n}$ represent the loadings of pollutant *i* in gridcell *n* from the intensive and extensive livestock sectors, respectively. $LivPop_{y,n}$ is the livestock population in gridcell *n* per livestock type *y*, with 8 livestock types considered (buffalo, chicken, cow, duck, goat, horse, pig, sheep), $E_{liv,y,i,n}$ is the per stock excretion rate of pollutant *i* (BOD in g stock^{-1} day^{-1}; FC in cfu stock^{-1} day^{-1}) of livestock type *y* and gridcell *n*, s_n is the fraction surface runoff in gridcell *n* and $R_{liv,i,n}$is removal fractions of pollutant *i* due to livestock waste management practices in gridcell *n* (Jones et al., 2021; Jones et al., 2022).

Gridded livestock numbers at 5 arc-minutes are from a global dataset for the reference year of 2010 (Gilbert et al., 2018). For the quantification of past gridded livestock numbers, a region-specific constant percentage growth in the number of animals per livestock type is applied to all grid cells based on data from the FAO (Thomson, 2003) (Table S5).

Table S5. Annual growth in livestock type (population number) between 1999 – 2030 (%), applied to gridded livestock populations for 1980 - 2015(Thomson, 2003)

Region	Livestock Type (annual growth %)				
	Cattle & Buffalo	Sheep & Goats	Pigs	Horses	Chickens & Ducks
North America	-0.1	0.2	0.1	0	0.6
Latin America & Caribbean	1	0.6	1.1	0	1.9
Western Europe	-0.1	0.2	0.1	0	0.6
Middle East & North Africa	1.5	1	0	0	2.1
Sub-Saharan Africa	1.1	1.2	1.4	0	2.2
Southern Asia	0.3	1.1	1	0	3.6
Eastern Europe & Central Asia	1.2	1.2	0.8	0	1.5
East Asia & Pacific	1.2	1.2	0.8	0	1.5

Excretion rates of BOD (Table S6) and FC (Table S7) per livestock type *y* and per region were determined through literature study, as per previous global water quality modelling studies (UNEP, 2016; Van Vliet et al., 2021). Excretion rates of pollutants per livestock type is assumed constant throughout the study period.

Table S6. Biological Oxygen Demand (BOD) loadings per animal per livestock type and geographic region (i.e. manure).

Region	Biological Oxygen Demand (g stock^{-1} day^{-1})*							
	Buffalo	Chicken	Cow	Duck	Goat	Horse	Pig	Sheep
Western Europe	400	8.3	400	8.3	50	300	233	50
Sub-Saharan Africa	240	8.3	240	8.3	50	300	186.4	35
Southern Asia	200	8.3	200	8.3	50	300	233	35
North America	400	8.3	400	8.3	50	300	233	50
Middle East & North Africa	280	8.3	280	8.3	50	300	186.4	35
Latin America & Caribbean	280	8.3	280	8.3	50	300	233	35
Eastern Europe & Central Asia	240	8.3	240	8.3	50	300	233	35
East Asia & Pacific	280	8.3	280	8.3	50	300	233	35

* as per Robinson et al., (2011), Wen et al., (2017), Vigiak et al., (2019), van Vliet et al., (2021).

Table S7. Fecal coliform (FC) loadings per animal per livestock type and geographic region (i.e. manure).

Region	Fecal coliform (cfu stock^{-1} day^{-1})*							
	Buffalo	**Chicken**	**Cow**	**Duck**	**Goat**	**Horse**	**Pig**	**Sheep**
Western Europe	$1.01 \cdot 10^{11}$	$1.36 \cdot 10^{8}$	$1.01 \cdot 10^{11}$	$2.43 \cdot 10^{9}$	$1.20 \cdot 10^{9}$	$1.40 \cdot 10^{9}$	$1.08 \cdot 10^{10}$	$1.12 \cdot 10^{9}$
Sub-Saharan Africa	$6.06 \cdot 10^{10}$	$1.36 \cdot 10^{8}$	$6.06 \cdot 10^{10}$	$2.43 \cdot 10^{9}$	$1.20 \cdot 10^{9}$	$1.40 \cdot 10^{9}$	$8.64 \cdot 10^{9}$	$7.84 \cdot 10^{8}$
Southern Asia	$5.05 \cdot 10^{10}$	$1.36 \cdot 10^{8}$	$5.05 \cdot 10^{10}$	$2.43 \cdot 10^{9}$	$1.20 \cdot 10^{9}$	$1.40 \cdot 10^{9}$	$1.08 \cdot 10^{10}$	$7.84 \cdot 10^{8}$
North America	$1.01 \cdot 10^{11}$	$1.36 \cdot 10^{8}$	$1.01 \cdot 10^{11}$	$2.43 \cdot 10^{9}$	$1.20 \cdot 10^{9}$	$1.40 \cdot 10^{9}$	$1.08 \cdot 10^{10}$	$1.12 \cdot 10^{9}$
Middle East & North Africa	$7.07 \cdot 10^{10}$	$1.36 \cdot 10^{8}$	$7.07 \cdot 10^{10}$	$2.43 \cdot 10^{9}$	$1.20 \cdot 10^{9}$	$1.40 \cdot 10^{9}$	$8.64 \cdot 10^{9}$	$7.84 \cdot 10^{8}$
Latin America & Caribbean	$7.07 \cdot 10^{10}$	$1.36 \cdot 10^{8}$	$7.07 \cdot 10^{10}$	$2.43 \cdot 10^{9}$	$1.20 \cdot 10^{9}$	$1.40 \cdot 10^{9}$	$1.08 \cdot 10^{10}$	$7.84 \cdot 10^{8}$
Eastern Europe & Central Asia	$6.06 \cdot 10^{10}$	$1.36 \cdot 10^{8}$	$6.06 \cdot 10^{10}$	$2.43 \cdot 10^{09}$	$1.20 \cdot 10^{9}$	$1.40 \cdot 10^{9}$	$1.08 \cdot 10^{10}$	$7.84 \cdot 10^{8}$
East Asia & Pacific	$7.07 \cdot 10^{10}$	$1.36 \cdot 10^{8}$	$7.07 \cdot 10^{10}$	$2.43 \cdot 10^{9}$	$1.20 \cdot 10^{9}$	$1.40 \cdot 10^{9}$	$1.08 \cdot 10^{10}$	$7.84 \cdot 10^{8}$

* as per Weaver et al., (2005) and Wilcock et al., (2006)

1.5 Irrigation

$$L_{irr,i,n} = RF_{irr,i,n} \cdot C_{irr,i,n} \quad \textbf{[5]}$$

The only pollutant considered from the irrigation sector in DynQual is TDS. To calculate TDS from the irrigation sector, the return flows from the irrigation sector in gridcell n ($RF_{irr,n}$ in $m^3\ s^{-1}$) is multiplied by a mean irrigation drainage concentration ($C_{irr,i,n}$) for pollutant i, which for TDS is in mg l^{-1} [5]. As irrigation runoff is rarely collected or treated (Wwap, 2017), no abation due to wastewater management practices occurs.

Irrigation return flows are simulated by PCR-GLOBWB 2, under the assumption that withdrawn water that is not consumed (via plant transpiration and open water or soil evaporation) is lost via percolation and contributes to groundwater recharge (Sutanudjaja et al., 2018). Mean irrigation drainage concentrations are derived from the electrical conductivity (dS m^{-1}) averaged over the topsoil (0-30cm) and subsoil (30-100cm) at 0.5^0 resolution from the ISRIC-WISE global soil database (Batjes, 2005), as per VIC-QUAL (Van Vliet et al., 2021). Electrical conductivity (EC) is converted to TDS using a TDS/EC ratio for freshwater of 0.65 (Walton, 1989). Mean irrigation drainage concentration is assumed to be constant throughout the study period.

1.6 Thermoelectric power

The only pollutant considered from the thermoelectric power sector is water temperature (Tw). Thermal pollution (heat dumps) from the power sector [6] is calculated based on a spatially-explicit powerplant database containing 13,506 powerplants with detailed information on fuel type and cooling type, representing an estimated 87% of the global thermoelectric capacity in 2015 (Lohrmann et al., 2019).

$$L_{pow,i,n} = \rho_w \cdot C_p \cdot RF_{pow,n} \cdot \Delta T_{pow\_rf} \quad \textbf{[6]}$$

Where $L_{pow,i,n}$ is the heat dump from thermo-electric powerplants [W] in gridcell n, C_p is the specific heat capacity of water [4,190 J kg^{-1} K^{-1}], ρ_w is the density of fresh water [1000 kg m^{-3}], $RF_{pow,n}$ is the return flows of cooling water [m^3 s^{-1}] in gridcell n and ΔT_{pow_rf} is the difference in water temperature between the return flows and ambient river water [K].

Water withdrawals and consumption per powerplant are from a spatially explicit powerplant dataset (Lohrmann et al., 2019). These estimates are quantified as a function of plant capacity, load hours and water use intensity, which depends primarily on fuel type and cooling system. The dataset considers five types of cooling systems (wet cooling towers, dry cooling systems, inlet cooling systems, once through cooling and recirculating cooling-pond systems) and four fuel types (nuclear, coal, gas and oil). Power return flows (RF_{pow}) are subsequently calculated by subtracting water consumption from the water withdrawal. We aggregated these power return flows at the gridcell level and delineate them in time based upon the construction year of the powerplant. The construction year is derived by cross-referencing powerplant coordinates with information from various other sources (http://GlobalEnergyObservatory.org/; https://datasets.wri.org/dataset/globalpowerplantdatabase).

A range of values for ΔT_{pow_rf} were found in the literature, varying from between 3 K based upon maximum permissible limits for powerplants in the US as per the Clean Water Act (Van Vliet et al., 2012) to 10 K from once-through systems in the USA in summer months between 2001-2005 (Madden et al., 2013). We selected an intermediate value of 7 K for ΔT_{pow_rf}, as this falls within the range of reported values in the literature and matches well with more recent global thermal emission rates of ~480 GW (Raptis et al., 2016). Results of a sensitivity analysis also suggests that values for ΔT_{pow_rf} of between 3 – 7 K have relatively moderate impacts on simulated water temperature in thermally polluted basins (Van Vliet et al., 2012).

1.7 Combined sectoral pollutant loadings

Combined loadings per water quality constituent are calculated by aggregating loadings from all contributing sectors [7].

$$L_{TDS,n} = L_{dom,TDS,n} + L_{man,TDS,n} + L_{usr,TDS,n} + L_{irr,TDS,n}$$

$$L_{BOD,n} = L_{dom,BOD,n} + L_{man,BOD,n} + L_{usr,BOD,n} + L_{intLiv,BOD,n} + L_{extLiv,BOD,n}$$

$$L_{FC,n} = L_{dom,FC,n} + L_{man,FC,n} + L_{usr,FC,n} + L_{intLiv,FC,n} + L_{extLiv,FC,n}$$

$$L_{Tw,n} = L_{pow,Tw,n} \quad \textbf{[7]}$$

Where, in each gridcell n, $L_{Tw,n}$ is the local Tw load [MW], $L_{TDS,n}$ is the local TDS load [g day^{-1}], $L_{BOD,n}$ is the local BOD load [g day^{-1}] and $L_{FC,n}$ is the local FC load [cfu day^{-1}].

2. Implementation of water quality equations

DynQual uses a numerical scheme (time-explicit fine differences) to simulate the routing of both water and pollutants through the surface water network (based on a local drain direction map), including in-stream processes, with a sub-daily timestep.

The length of the time interval (Δt_n in seconds) is estimated with respect to both channel storage and discharge [8]. This ensures that the length of the time interval is small enough to ensure that flow from gridcell *n* only flows into the immediately downstream gridcell *n+1*, and not further (i.e. $\Delta t_n > T_n$, where T_n represents the residence time of gridcell *n*).

$$\Delta t_n = \frac{h_n \cdot A_n \cdot \left(\frac{w_n \cdot l_n}{A_n}\right)}{Q_n} \quad \textbf{[8]}$$

Where h_n is the water height (m), A_n is the gridcell area (m^2), w_n is the channel width (m), l_n is the channel length (m) and Q_n is the discharge ($m^3\ s^{-1}$) simulated at the sub-daily timestep using the simplified kinematic wave routing, all in gridcell *n*.

While Δt_n is initially determined per individual gridcell, the shortest calculated interval is used consistently for all gridcells within the simulation extent (Δt). We also set a maximum time-interval (Δt) of 720s (i.e. to ensure routing procedure happens at least once every 12 minutes). While we could further increase the numerical accuracy of our simulations by introducing shorter time intervals, this also increases computational times, and thus a balance must be struck (Loucks and Beek, 2017). More information on the implementation of water quality equations within DynQual is available in the open-access model code (https://github.com/UU-Hydro/DYNQUAL).

3. Model validation

Tw and BOD data was downloaded from the Global River Water Quality Archive (GRQA) (Virro et al., 2021), which aggregates data from a variety of datasets including GEMStat (Global Freshwater Quality Database) (UNEP, 2020), GLORICH (GLObal River CHemistry) (Hartmann et al., 2014) and WQP (Water Quality Portal) (Read et al., 2017). Electrical conductivity (EC) data was obtained from a global surface water database (Thorslund and Van Vliet, 2020), which we additionally supplemented with GEMStat data (UNEP, 2020), and converted to TDS using a conversion factor of 0.7 (Walton, 1989). FC data was obtained from GEMStat (UNEP, 2020), additionally supplemented with data from the National Water Information System (NWIS) from the United States Geological Survey (USGS) (U.S. Geological Survey, 2016). The number of water quality modelling stations and associated observations used for validation of DynQual is presented in Table S8.

Table S8. Number of water quality monitoring stations and measurements used for DynQual validation.

Water quality constituent	Number of monitoring stations	Number of observations
Water Temperature (Tw)	7,516	750,112
Total Dissolved Solids (TDS)	27,238	7,473,916
Biological Oxygen Demand (BOD)	2,710	230,444
Fecal Coliform (FC)	2,235	210,664

The spatial distribution in root mean square error normalised by the mean (nRMSE) [9], combined with two example time-series plots comparing observations with model simulations where data availability was high, are displayed for Tw (Figure S2), TDS (Figure S3), BOD (Figure S4) and FC (Figure S5).

$$nRMSE = \frac{\sqrt{\frac{\sum_{i=1}^{N} (Sim_i - Obs_i)}{n}}}{\bar{O}bs} \quad \textbf{[9]}$$

Overall, calculated nRMSE values indicate reasonable mode performance. In accordance with previous studies, the best model performance is found for Tw, followed by TDS, BOD and FC respectively (UNEP, 2016; Van Vliet et al., 2021; Jones et al., 2022). In general, best model performance for all water quality constituents is found at monitoring stations with higher discharge, whereby model performance for hydrological variables (e.g. discharge) also tends to be higher (Sutanudjaja et al., 2018).

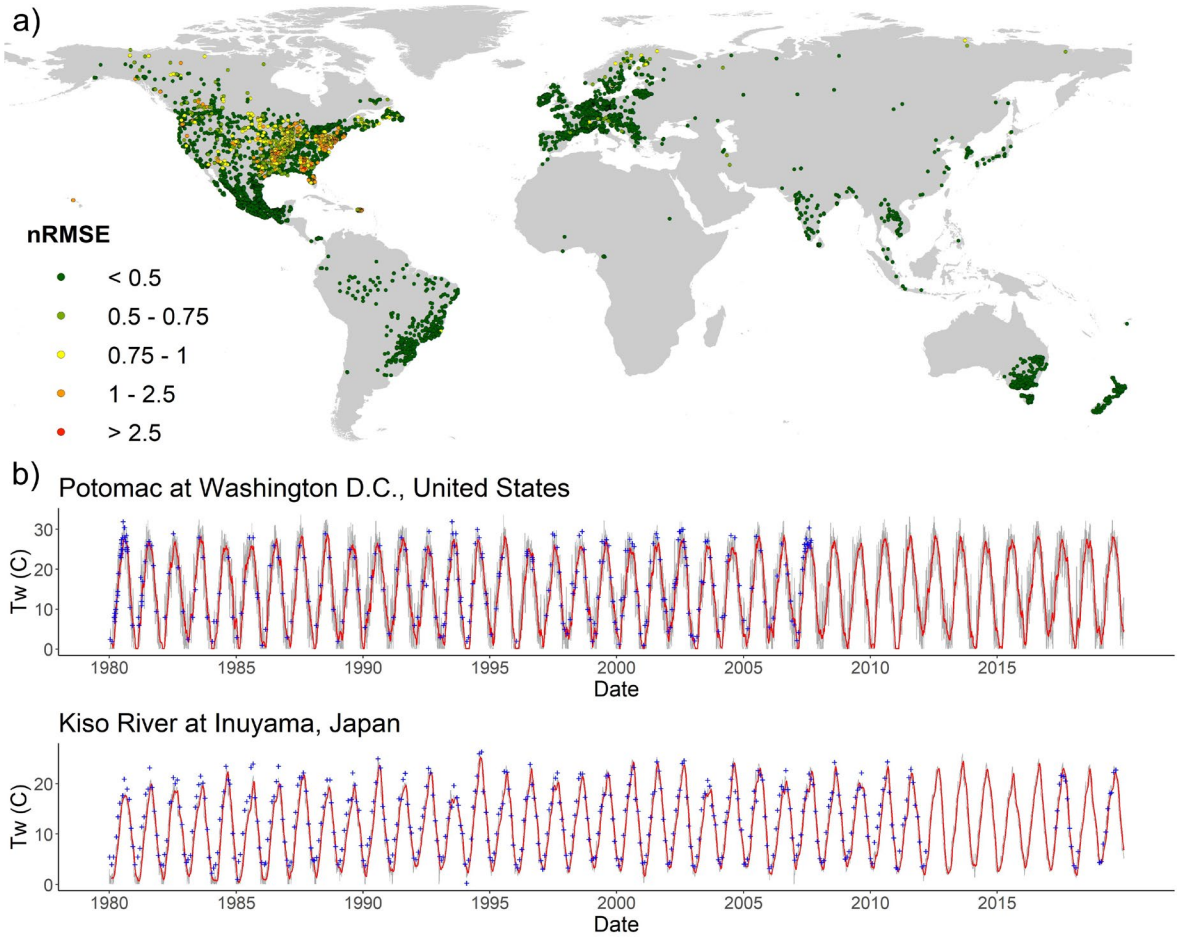

Figure S2. Spatial patterns in normalised root mean square error of water temperature (Tw) at all validation sites (a), with time-series displaying observed vs. simulated results at stations with high data availability (b) from 1980 - 2019. Observed Tw is indicated by blue crosses, simulated daily Tw by grey lines and 30-day running average Tw by red lines.

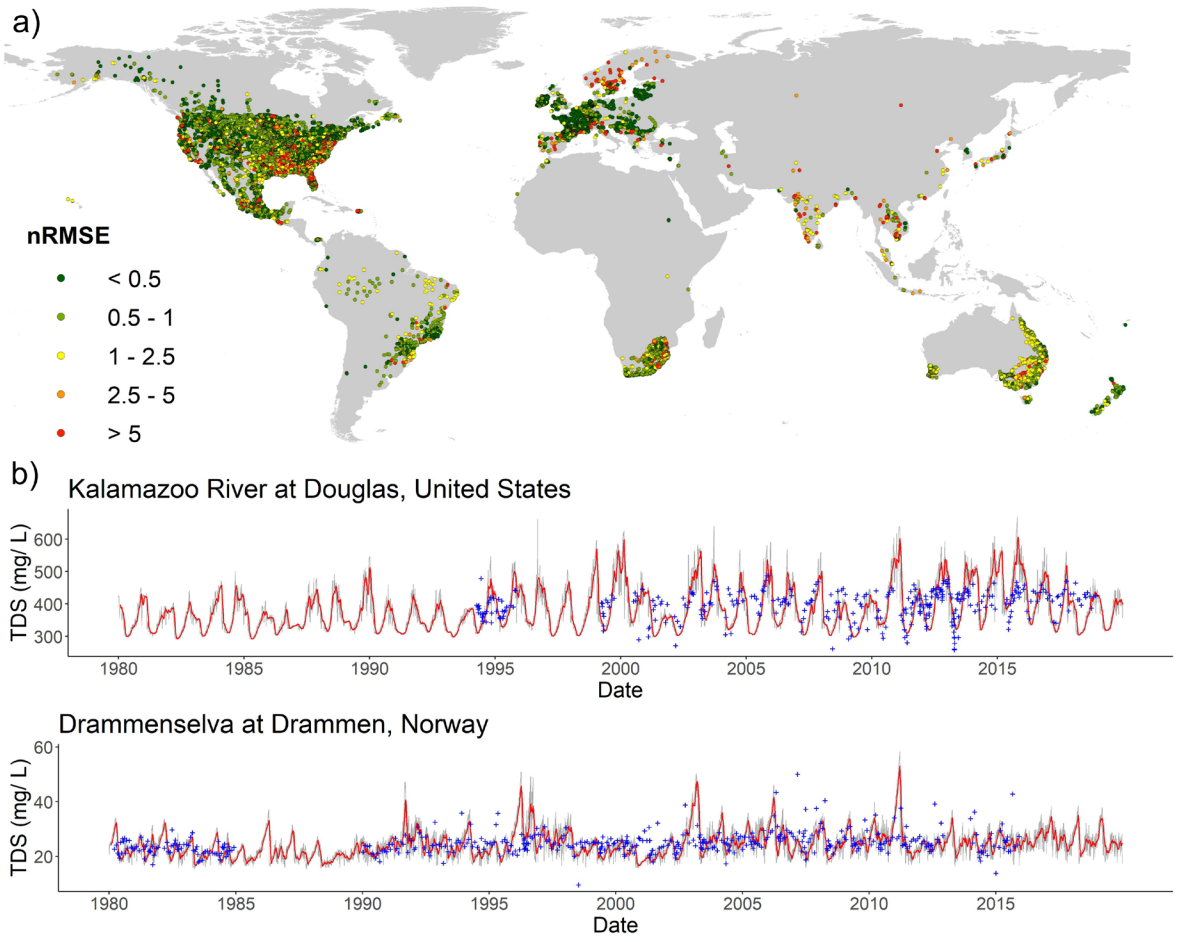

Figure S3. Spatial patterns in normalised root mean square error of total dissolved solids (TDS) concentrations at all validation sites (a), with time-series displaying observed vs. simulated results at stations with high data availability (b) from 1980 - 2019. Observed TDS is indicated by blue crosses, simulated daily TDS by grey lines and 30-day running average TDS by red lines.

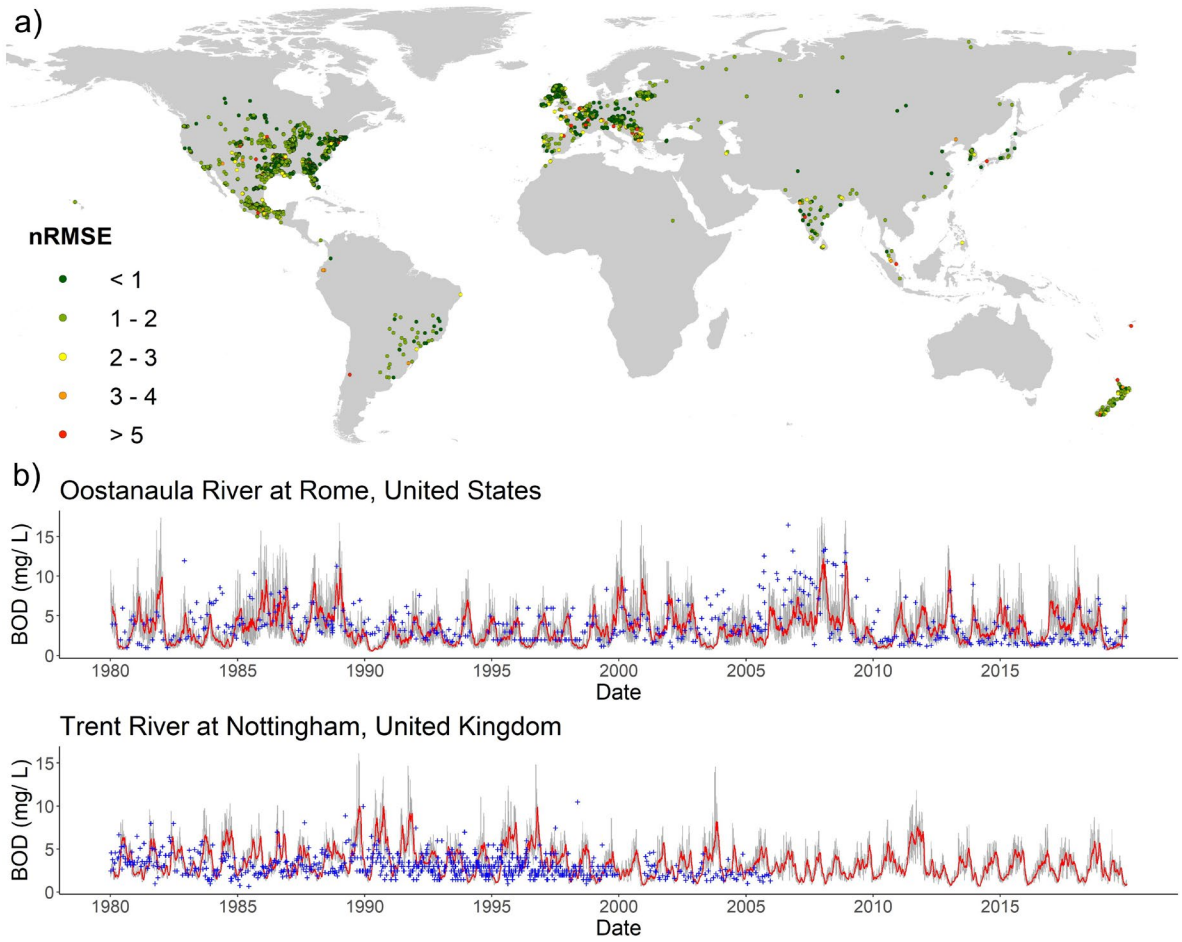

Figure S4. Spatial patterns in normalised root mean square error of biological oxygen demand (BOD) concentrations at all validation sites (a), with time-series displaying observed vs. simulated results at stations with high data availability (b) from 1980 - 2019. Observed BOD is indicated by blue crosses, simulated daily BOD by grey lines and 30-day running average BOD by red lines.

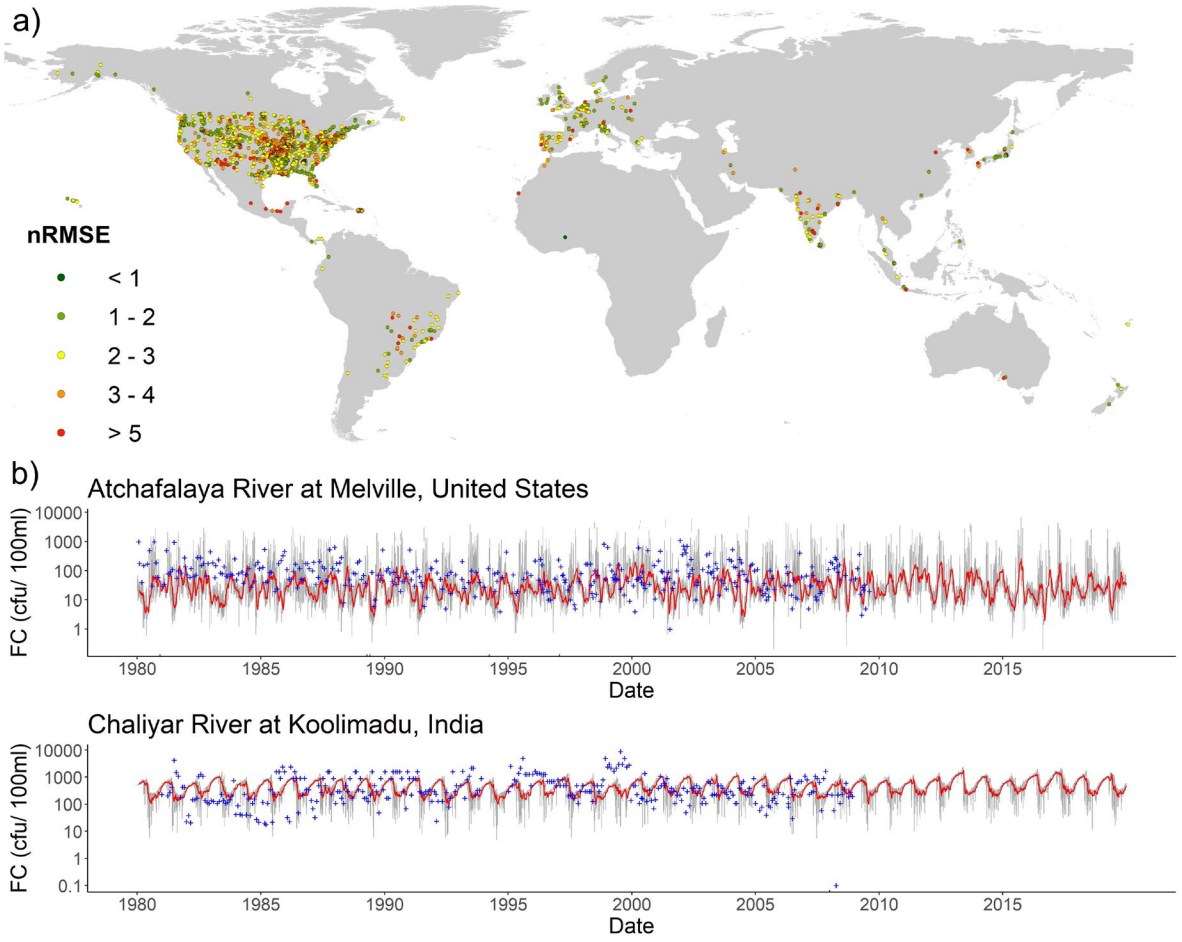

315 **Figure S5.** Spatial patterns in normalised root mean square error of fecal coliform (FC) concentrations at all validation sites (a), with time-series displaying observed vs. simulated results at stations with high data availability (b) from 1980 - 2019. Observed FC is indicated by blue crosses, simulated daily FC by grey lines and 30-day running average FC by red lines.

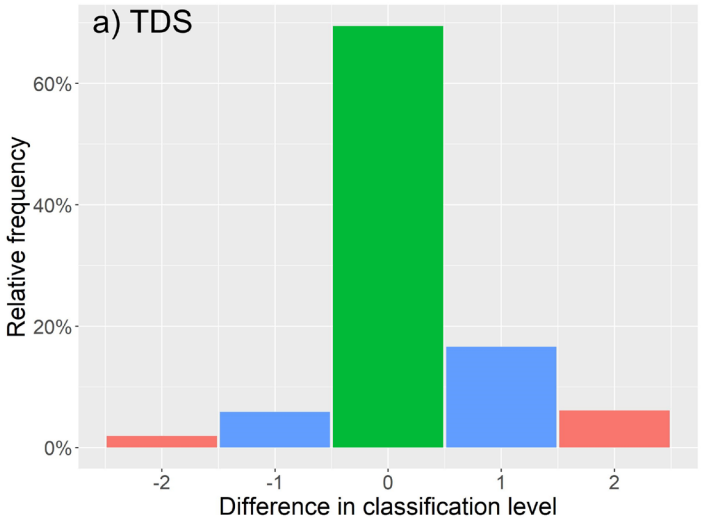

Pollutant status	Total dissolved solids (TDS; mg l^{-1})
Low	< 525
Medium	525 – 2100
High	> 2100

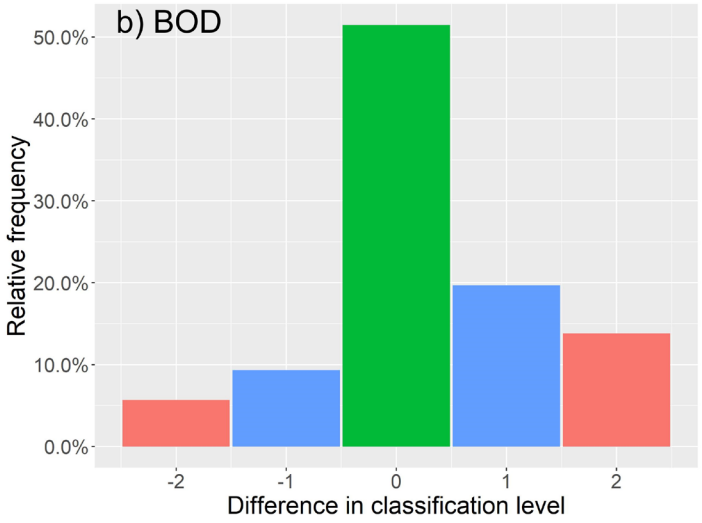

Pollutant status	Biological oxygen demand (BOD; mg l^{-1})
Low	< 4
Medium	4 – 8
High	> 8

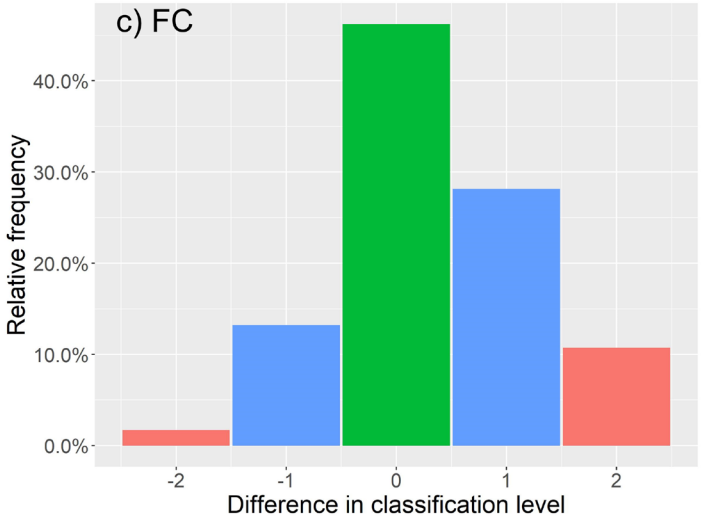

Pollutant status	Fecal coliform (FC; cfu $100ml^{-1}$)
Low	< 100
Medium	100 – 1000
High	> 1000

320

Figure S6. Differences in observed vs simulated pollutant classes for a) total dissolved solids (TDS), b) biological oxygen demand (BOD) and c) fecal coliform (FC). Pollutant classes are defined based on water use and ecological limitations, as stated by governmental and international organisations. A difference in classification level of "0" indicates the simulated pollutant class matches the observed
325 pollutant class, while negative differences indicate that observed concentrations exceeded simulated concentrations, and vice-versa for positive differences.

References

Batjes, N. H.: ISRIC-WISE global data set of derived soil properties on a 0.5 by 0.5 degree grid (Version 3.0). World Soil Information, Wageningen, 24, 2005.

Gilbert, M., Nicolas, G., Cinardi, G., Van Boeckel, T. P., Vanwambeke, S. O., Wint, G. R. W., and Robinson, T. P.: Global distribution data for cattle, buffaloes, horses, sheep, goats, pigs, chickens and ducks in 2010, Scientific Data, 5, 180227, 10.1038/sdata.2018.227, 2018.

Hartmann, J., Lauerwald, R., and Moosdorf, N.: A Brief Overview of the GLObal RIver Chemistry Database, GLORICH, Procedia Earth and Planetary Science, 10, 23-27, https://doi.org/10.1016/j.proeps.2014.08.005, 2014.

Jones, E. R., van Vliet, M. T. H., Qadir, M., and Bierkens, M. F. P.: Country-level and gridded estimates of wastewater production, collection, treatment and reuse, Earth Syst. Sci. Data, 13, 237-254, 10.5194/essd-13-237-2021, 2021.

Jones, E. R., Bierkens, M. F. P., Wanders, N., Sutanudjaja, E. H., van Beek, L. P. H., and van Vliet, M. T. H.: Current wastewater treatment targets are insufficient to protect surface water quality, Communications Earth & Environment, 3, 221, 10.1038/s43247-022-00554-y, 2022.

Lange, S. and Geiger, T.: ISIMIP3a population input data (1.0) [dataset], 10.48364/ISIMIP.822480, 2020.

Lohrmann, A., Farfan, J., Caldera, U., Lohrmann, C., and Breyer, C.: Global scenarios for significant water use reduction in thermal power plants based on cooling water demand estimation using satellite imagery, Nature Energy, 4, 1040-1048, 10.1038/s41560-019-0501-4, 2019.

Loucks, D. P. and Beek, E. v.: Water quality modeling and prediction, in: Water resource systems planning and management, Springer, 417-467, 2017.

Madden, N., Lewis, A., and Davis, M.: Thermal effluent from the power sector: an analysis of once-through cooling system impacts on surface water temperature, Environmental Research Letters, 8, 035006, 10.1088/1748-9326/8/3/035006, 2013.

Raptis, C. E., van Vliet, M. T. H., and Pfister, S.: Global thermal pollution of rivers from thermoelectric power plants, Environmental Research Letters, 11, 104011, 10.1088/1748-9326/11/10/104011, 2016.

Read, E. K., Carr, L., De Cicco, L., Dugan, H. A., Hanson, P. C., Hart, J. A., Kreft, J., Read, J. S., and Winslow, L. A.: Water quality data for national-scale aquatic research: The Water Quality Portal, Water Resources Research, 53, 1735-1745, https://doi.org/10.1002/2016WR019993, 2017.

Robinson, T. P., Thornton, P. K., Franceschini, G., Kruska, R., Chiozza, F., Notenbaert, A. M. O., Cecchi, G., Herrero, M. T., Epprecht, M., and Fritz, S.: Global livestock production systems, Food and Agriculture Organization of the United Nations (FAO) and International Livestock Research Institute (ILRI), Rome, 152 pp pp.2011.

Sutanudjaja, E., Beek, R., Wanders, N., Wada, Y., Bosmans, J., Drost, N., Ent, R., de Graaf, I., Hoch, J., de Jong, K., Karssenberg, D., López, P., Pessenteiner, S., Schmitz, O., Straatsma, M., Vannametee, E., Wisser, D., and Bierkens, M.: PCR-GLOBWB 2: A 5 arcmin global hydrological and water resources model, Geoscientific Model Development, 11, 2429-2453, 10.5194/gmd-11-2429-2018, 2018.

Thomson, K.: World agriculture: towards 2015/2030: an FAO perspective: Jelle Briunsma (Ed.), FAO/Earthscan, 2003. 432 pp. ISBNs: 92 5 104835 5 (FAO paperback), 1 84407 007 7 (Earthscan

paperback) and 1 84407 008 57 (Earthscan hardback), Land Use Policy, 20, 375, 10.1016/S0264-8377(03)00047-4, 2003.

Thorslund, J. and van Vliet, M. T. H.: A global dataset of surface water and groundwater salinity measurements from 1980–2019, Scientific Data, 7, 231, 10.1038/s41597-020-0562-z, 2020.

U.S. Geological Survey: National Water Information System data available on the World Wide Web (USGS Water Data for the Nation) [dataset], http://dx.doi.org/10.5066/F7P55KJN, 2016.

UNEP: A Snapshot of the World's Water Quality: Towards a global assessment, United Nations Environment Programme, Nairobi, Kenya, 162pp, 2016.

UNEP: GEMStat database of the Global Environment Monitoring System for Freshwater (GEMS/Water) Programme., 2020.

van Vliet, M., Yearsley, J., Ludwig, F., Vögele, S., Lettenmaier, D., and Kabat, P.: Vulnerability of US and European Electricity Supply to Climate Change, Nature Climate Change, 2, 676-681, 10.1038/nclimate1546, 2012.

van Vliet, M. T. H., Jones, E. R., Flörke, M., Franssen, W. H. P., Hanasaki, N., Wada, Y., and Yearsley, J. R.: Global water scarcity including surface water quality and expansions of clean water technologies, Environmental Research Letters, 16, 024020, 10.1088/1748-9326/abbfc3, 2021.

Vigiak, O., Grizzetti, B., Udias-Moinelo, A., Zanni, M., Dorati, C., Bouraoui, F., and Pistocchi, A.: Predicting biochemical oxygen demand in European freshwater bodies, Science of The Total Environment, 666, 1089-1105, https://doi.org/10.1016/j.scitotenv.2019.02.252, 2019.

Virro, H., Amatulli, G., Kmoch, A., Shen, L., and Uuemaa, E.: GRQA: Global River Water Quality Archive, Earth Syst. Sci. Data, 13, 5483-5507, 10.5194/essd-13-5483-2021, 2021.

Walton, N. R. G.: Electrical Conductivity and Total Dissolved Solids—What is Their Precise Relationship?, Desalination, 72, 275-292, https://doi.org/10.1016/0011-9164(89)80012-8, 1989.

Wen, Y., Schoups, G., and van de Giesen, N.: Organic pollution of rivers: Combined threats of urbanization, livestock farming and global climate change, Scientific Reports, 7, 43289, 10.1038/srep43289, 2017.

Williams, R., Keller, V., Voß, A., Bärlund, I., Malve, O., Riihimäki, J., Tattari, S., and Alcamo, J.: Assessment of current water pollution loads in Europe: estimation of gridded loads for use in global water quality models, Hydrological Processes, 26, 2395-2410, https://doi.org/10.1002/hyp.9427, 2012.

WWAP: The United Nations World Water Development Report 2017. Wastewater: The Untapped Resource, Paris, UNESCO, 2017.